Article title: Phosphorylation of the exocyst subunit Exo70B2 contributes to the regulation of its function

Authors: Ooi-Kock Teh[1,2,3], Chil-Woo Lee[1,4], Franck Aniset Ditengou[5], Till Klecker[6], Giulia Furlan[1], Marco Zietz[1], Gerd Hause[7], Lennart Eschen-Lippold[1], Wolfgang Hoehenwarter[1], Justin Lee[1], Thomas Ott[5], Marco Trujillo[1]

[1]Leibniz Institute of Plant Biochemistry, Halle (Saale) 06120, Germany

[2]Present address: Institute for International Collaboration, Hokkaido University, Sapporo 060-0815, Japan

[3]Department of Biological Science, School of Science, Hokkaido University, 060-0810, Japan

[4]Present address: Korea Honey Bee Disease Institute, Gyeonggi-do, 16227, Korea

[5]Institute of Cell Biology, University of Freiburg, 79104 Freiburg, Germany

[6]Institute of Cell Biology, University of Bayreuth, 95440 Bayreuth, Germany

[7]Biozentrum, Martin-Luther-University Halle-Wittenberg, Halle (Saale) 06120, Germany

Author for correspondence: Marco Trujillo, Leibniz Institute of Plant Biochemistry, Halle (Saale) 06120, Germany, Email: mtrujillo@ipb-halle.de , phone: +49 (0) 345-5582-1720, fax: +49 (0) 345-5582-1709

Abstract

The exocyst is a conserved hetero-octameric complex mediating early tethering during exocytosis. Its Exo70 subunit plays a critical role as a spatiotemporal regulator by mediating numerous protein and lipid interactions. However, a molecular understanding of the exocyst function remains challenging. We show that Exo70B2 locates to dynamic foci at the plasma membrane and transits through a BFA-sensitive compartment, reflecting its canonical function in secretion. However, treatment with the salicylic acid (SA) defence hormone analogue Benzothiadiazole (BTH), or the immunogenic peptide flg22, induced Exo70B2 transport into the vacuole. We uncovered two ATG8-interacting motifs (AIMs) located in the C-terminal domain (C-domain) that mediate its recruitment into the vacuole. Moreover, we also show that Exo70B2 is phosphorylated near the AIMs and mimicking phosphorylation enhanced ATG8 interaction. Finally, Exo70B2 phosphonull lines were hypersensitive to BTH and more resistant to avirulent bacteria which induce SA production. Our results suggest a molecular mechanism in which phosphorylation of Exo70B2 by MPK3 functions in a feed-back system linking cellular signalling to the secretory pathway.

Introduction

The exocyst is an evolutionary conserved protein complex implicated in the tethering of secretory vesicles to the plasma membrane (PM) before SNARE-mediated membrane fusion. The first exocyst components were described in yeast as temperature sensitive mutants in which vesicles accumulated due to failed fusion to the PM (Novick et al., 1980). All subunits of the exocyst were later shown to work in a complex and to mediate exocytosis of post-Golgi vesicles (Wu and Guo, 2015). The complex was subsequently found to be conserved in plants, and the first reported mutant phenotypes supported the anticipated function in secretion (Cole et al., 2005; Wen et al., 2005). However, in contrast to all other eukaryotic organisms, the Exo70 subunit has experienced a substantial expansion into many paralogues; 23 in *Arabidopsis thaliana* (referred to as Arabidopsis) and 47 in rice (Cvrckova et al., 2012).

The secretory pathway mediates the transport of lipids and proteins to the PM. Specific conditions such as active growth and infection, engage the secretory pathway and significantly enhance its activity (Wang et al., 2005). During the immune response de-novo synthesis of a vast array of proteins is induced, including PM-localized receptors and proteins with antimicrobial activities which are delivered to the extracellular space (Gu et al., 2017). The defence hormone SA plays a key function by coordinately upregulating the secretory pathway (Wang et al., 2005; Tateda et al., 2014).

Localization of Exo70 in humans and yeast to the PM is mediated by its ability to bind phosphatidylinositol 4,5-bisphosphate ($PI(4,5)P_2$) (He et al., 2007a; Liu et al., 2007). Although direct membrane binding of an exocyst component has not been shown in plants, the small molecule

Endosidin2 (ES2) binds to Exo70A1 and inhibits its exocytosis and recycling (Zhang et al., 2016). Residues contributing to ES2 binding were located in the C-domain of Exo70A1 at the C-terminus, suggesting that the membrane-binding function of the C-terminal region is conserved in plants.

The exocyst has been shown to play a role in the immune response of both plants and animals. The Sec5 subunit forms an effector complex with GTPase RalB and directly recruits and activates the atypical IκB kinase family member TBK1 in human cells (Chien et al., 2006). The RalB/Sec5 complex contributes to the activation of the innate immune response via TBK1 in response to virus infection. In plants, a function in immunity has mainly been reported for Exo70 homologues. Mutants of *Exo70B2* and *Exo70H1* are more susceptible to virulent bacterial pathogens (Pecenkova et al., 2011; Stegmann et al., 2012). Moreover, Exo70B2 was shown to be required for full activation of pathogen-associated molecular pattern (PAMP)-triggered immunity (PTI) (Stegmann et al., 2012). For Exo70B1, the closest homologue of Exo70B2, there have been contrasting reports regarding its function in the resistance against the bacterial pathogen *Pseudomonas syringae* pv *tomato* DC3000 (Stegmann et al., 2012; Stegmann et al., 2013; Zhao et al., 2015).

Although the canonical function of the exocyst is exocytosis, it has been implicated in other processes (Wu and Guo, 2015). Exo70B1 is transported into the vacuole and partially colocalizes with ATG8, a ubiquitin-like protein required for the formation of autophagosomal membranes (Kulich et al., 2013). Mutants of *exo70B1* also displayed reduced accumulation of anthocyanins and spontaneous cell death reminiscent of autophagy-deficient mutants (Kulich et al., 2013). This has led to the assumption that Exo70B1 plays a general function in autophagy. The Exo70E2 homologue is recruited to autophagosomes after autophagy induction by BTH (Lin et al., 2015). However, under control conditions it remained in distinct compartments. In human cells, RalB directly binds to Exo84, inducing the assembly of catalytically active ULK1 and Beclin1-VPS34 complexes on the exocyst to drive autophagosome formation (Bodemann et al., 2011).

A possible explanation for the different functions of the exocyst is that many cellular processes need to be coordinated with exocyst-mediated exocytosis (Wu and Guo, 2015). Therefore, exocyst activity must to be tightly coordinated to allow temporal and spatial control of its functions.

In mammals, the mitogen-activated protein kinase ERK1/2 phosphorylates Exo70 in response to epidermal growth factor (EGF), resulting in the assembly of the exocyst complex and secretion (Ren and Guo, 2012). Adding another regulatory layer, we previously showed that upon activation of PTI, Exo70B2 was targeted by the E3 ligase PUB22 for degradation during the immune response (Stegmann et al., 2012; Furlan et al., 2017).

In this study, we show that part of the cellular Exo70B2 pool is localized to the PM, and in contrast to other exocyst subunits, transits through a BFA-sensitive compartment. Treatment with the SA analogue BTH induces the accumulation of Exo70B2 in the microsomal membrane fraction, which reflects its transport into the vacuole by autophagy. Exo70B2 can be phosphorylated by the PAMP-

responsive MPK3, and plants expressing a non-phosphorylatable version display enhanced sensitivity to BTH, as well as increased resistance to avirulent bacteria. The enhanced interaction of the Exo70B2 phosphomimic with ATG8 suggests that phosphorylation contributes to Exo70B2 degradation by autophagy, inhibiting its participation in exocytosis.

Results

Exo70B2 localizes to dynamic foci at the plasma membrane

In an effort to gain insight into exocyst function, and in particular of the Exo70B2 subunit, we characterized stable transgenic lines carrying the GFP-Exo70B2 fusion under control of the *UBQ10* promoter in the *exo70B2-3* background (Grefen et al., 2010). We opted to employ the *UBQ10* promoter, because lines under the control of a 1.5kbp fragment upstream of the *Exo70B2* CDS didn't lead to detectable expression, similarly to what was reported by Li et al. (Li et al., 2010).

GFP-Exo70B2 was detected in the cytoplasm of epidermal cells in cotyledon and roots, as well as a continuous cell-peripheral localization, which suggested PM localization (Figure 1A). To confirm PM localization, we plasmolysed cells using mannitol. GFP-Exo70B2 was detected at the periphery and in Hechtian strands of plasmolysed epidermal cells, suggesting that Exo70B2 localized to the PM (Figure 1B). To support our observations, we analysed the localization in root hairs which show tip growth, reasoning that GFP-Exo70B2 function would be focused to regions of high secretory activity (Honkanen and Dolan, 2016). High-resolution microscopy revealed that GFP-Exo70B2 localized to distinct foci at the periphery of in root hairs and the number of foci increased towards the tip where secretory activity is highest. The additional analysis by variable angle epifluorescence microscopy (VEAM)TIRF microscopy demonstrated that these foci are dynamic with a transient dwelling at the PM (Movie S1).

Treatment with BFA, which inhibits endosomal recycling of PM proteins, resulted in the accumulation of Exo70B2 in BFA-bodies, indicating that it transits through the *trans*-Golgi network (TGN) (Figure 1C). These results are consistent with a canonical function of Exo70B2 in the secretion of post-Golgi vesicles.

Exo70B2 is transported into the vacuole where it colocalizes with autophagic markers

We previously reported that Exo70B2 is targeted for degradation after activation of the immune response by the E3 ligase PUB22 (Stegmann et al., 2012). Ubiquitination of Exo70B2 by PUB22 suggested that it may be targeted for degradation via the proteasome. However, its association to the PM and accumulation in BFA-bodies indicated that Exo70B2 enters the endocytic, or alternate degradation pathways, capable of processing membrane-associated proteins. In support of such a scenario, studies in mammals have shown that exocyst participates in the activation of autophagy (Bodemann et al., 2011). Moreover, Exo70B1 and Exo70E2 colocalized with the autophagy marker

ATG8 upon tunicamycin or BTH treatment respectively, in plants (Ichimura et al., 2000; Kulich et al., 2013; Lin et al., 2015).

To induce autophagy we employed BTH (Yoshimoto et al., 2009; Lin et al., 2015), which is an analogue of the phytohormone SA, a central component of the immune response and induces the expression of hundreds of genes (Wang et al., 2005; Vlot et al., 2009). Inhibition of the vacuolar degradation by Concanamycin A (ConcA), revealed basal transport of Exo70B2 into the vacuole, reflected by the accumulation of punctae in the vacuole of elongated epidermal root cells, but not detectable in cotyledon cells (Figure 2A). By contrast, co-treatment with BTH induced the accumulation of intravacuolar punctae in both roots and cotyledons (Figure 2A). Analysis of Sec6, another subunit of the exocyst, showed that BTH had a similar effect and resulted in its delivery to the vacuole (Figure S1A).

Supporting the transport of Exo70B2 into the vacuole by autophagy, the marker proteins ATG8a and NBR1 colocalized to a subpopulation of punctae after BTH/ConcA treatment (Figure 2B) with Pearson's correlation coefficients of 0.48 for ATG8 and 0.4 for NBR1 (Figure 2C) (Kirkin et al., 2009; Svenning et al., 2011). Moreover, ultrastructural analysis confirmed that Exo70B2 was transported into the vacuole upon autophagy induction (Figure S1B).

To further dissect the behaviour of Exo70B2, we analysed the effect of BTH on protein levels. Analysis of total protein detected by immunoblot (IB) did not show obvious changes after BTH treatment, in spite of increased fluorescence intensity (Figure 2E, upper panel). Similarly, ConcA treatment, alone or in combination with BTH, resulted in only minor variations of Exo70B2 in total protein extracts.

Because BTH treatment remobilises Exo70B2 to the vacuole, we analysed protein fractions containing both soluble and microsomal proteins and lacking larger organelles such as nuclei and chloroplasts. In contrast to total protein, this fraction contained non-detectable levels of Exo70B2 in control samples (Figure 2E, lower panel). However, treatment with BTH and ConcA, alone or combined, resulted in increased amounts of Exo70B2. Moreover, GFP cleavage, which can be indicative of autophagy (Marshall et al., 2015), was observed for samples treated with ConcA, BTH and ConcA.

This fraction was further separated by ultracentrifugation, resulting in a microsomal pellet containing membrane-bound proteins, and a supernatant with soluble proteins. Comparison of equivalent samples amounts showed that while Exo70B2 was present in the microsomal fraction, it was not detectable as a soluble protein (Figure 2F). However, higher levels present in the total protein extract, also indicate additional populations of Exo70B2 (Figure 2F). Finally, we show that microsome-associated Exo70B2 increases upon BTH treatment (Figure 2G).

Taken together, BTH activates Exo70B2 transport into the vacuole potentially by autophagy, which is reflected by the colocalization with ARG8 and the remobilization of Exo70B2 sub-pools to membrane fractions.

Exo70B2 is transported into the vacuole upon activation of the immune response

Because we previously showed that Exo70B2 contributed to PTI (Stegmann et al., 2012), we tested the impact of activating the immune response. Treatment with flg22, which is perceived by the immune receptor FLS2, or ConcA alone, did not result in detectable changes (Figure 3A). However, flg22/ConcA co-treatment revealed the transport of Exo70B2 into the vacuole (Figure 3A). As previously shown, flg22 treatment resulted in the degradation of Exo70B2 (Figure 3B). To test whether this reflected vacuolar degradation, we pre-treated seedlings with ConcA. Inhibition of the vacuolar degradation reduced Exo70B2 degradation (Figure 3B).

Since flg22 treatment induced Exo70B2 transport into the vacuole, we wondered whether flg22 potentially increased autophagic flux. Treatment of seedlings with flg22, resulted in an increase of NBR1 protein levels, and flg22/ConcA co-treatment further enhanced this effect (Figure S2A). In accordance, NBR1 accumulated in the vacuole in response to flg22, and co-treatment with ConcA resulted in both a diffuse vacuolar signal and perivacuolar punctae (Figure S2B). These results are in agreement with a potential degradation of Exo70B2 by autophagy in response to the activation of the immune response.

Exo70B2 interacts with and is phosphorylated by MPK3 in vitro

Induction of Exo70B2 transport into the vacuole by flg22 treatment prompted us to search for a link to immune signalling. Exocyst subunits including Exo70B2 were reported to be significantly increased in phosphoprotein-enriched fractions of Arabidopsis plants expressing the constitutively active MKK5-DD variant in comparison to the kinase-inactive KR mutant: Exo70B2 by 2.28 fold (p value <0.001), Exo70E1 2.35 fold (p value <0.05) and Sec5A 2.86 fold (p value <0.05) (Lassowskat et al., 2014; Lee et al., 2015). FLS2 activation by flg22 induces the MKK5 branch of MAPKs, which includes MPK3 or MPK6 and other downstream kinases. Because MAPK signalling, and possibly autophagy, are induced during the immune response, we hypothesized that Exo70B2 may represent a link between these pathways.

To evaluate this possibility, we first assayed the interaction with MPK3, MPK4, MPK6, MPK8 and MPK11 using bimolecular fluorescence complementation (BiFC). We found that from the tested MAPKs, both MPK3 and MPK11 reconstituted fluorescence when transiently coexpressed with Exo70B2 (Figure 4A and Figure S3A). Although the BiFC results suggested that Exo70B2 also interacts with MPK11, the lack of specific MPK11 antibodies and the typically low activity of MPK11 (Bethke et al., 2012), impedes its analysis. Therefore, we decided to focus on MPK3, which was also shown to phosphorylate the E3 ligase PUB22, which targets Exo70B2's (Furlan et al., 2017). Confirming the interaction, endogenous MPK3 co-immunoprecipitated (IP) with Exo70B2 by anti-GFP antibodies in two independent homozygous lines (T3) carrying the *UBQ10prom-GFP-Exo70B2* construct in the *exo70B2-3* background (Figure 4B). The interaction was independent of flg22 treatment, suggesting that both proteins constitutively associate under the tested conditions. In vitro pull-down

experiments of bacterially expressed Exo70B2 and MPK3 showed that both proteins interacted directly, while MPK6 displayed only a weak interaction (Figure 4C).

Interaction between Exo70B2 and MPK3 opened the possibility that Exo70B2 is a substrate of MPK3. To test this, we carried out in vitro phosphorylation assays using purified recombinant MPK3, MPK4, MPK6 and MPK11. Consistent with the direct interaction, Exo70B2 was readily trans-phosphorylated by MPK3 but not by MPK4 or MPK6 (Figure 4D). In the case of MPK11, kinase activity of recombinant MPK11 is typically low in our hands, and consequently, no phosphorylation of Exo70B2 was detectable.

Recombinant Exo70B2 phosphorylated by MPK3 was next analysed by LC-MS/MS to determine the phosphorylation sites. We identified two residues, namely S554 and S567, both of which are located in the C-domain at the C-terminal portion of the protein (Figure 4E and Figure S3B). Both residues are followed by a proline, and thus represent typical MAPK phosphorylation motifs. No phosphopeptides were identified in controls without kinase. To confirm that the phosphorylation also takes place in vivo, we immunopurified GFP-Exo70B2 from transgenic seedlings treated with flg22 for 30 and 140 min and analysed samples by LC-MS/MS. Both phosphorylations in residues S554 and S567 could be identified, indicating that phosphorylation also takes place in vivo, while no phosphorylation was detected in non-treated samples (Figure S3C and Table S2). A sequence alignment between Exo70 homologues of the identified sites indicates that these residues are not conserved, suggesting a specialized regulatory function in Exo70B2 (Figure S3D).

Exo70B2 interaction with ATG8 through AIMs is increased in phosphomimic variant

Sequence analyses have predicted an over proportional presence of ATG8-interaction motifs (AIMs) in the Arabidopsis Exo70 family (Cvrckova and Zarsky, 2013; Tzfadia and Galili, 2013). We identified two putative AIMs located in the C-domain of Exo70B2: AIM1 508-DGPYPKL and AIM2 522-SQFDEV (Figure 5A).

We first tested the interaction by coexpressing Exo70B2 with ATG8f, which resulted in fluorescence complementation in a BiFC assay (Figure 5B and Figure S4A). To confirm that the interaction was mediated by the AIMs, we generated mutants in which we replaced YPKL (AIM1) and FDEV (AIM2) by APKA and ADEA, respectively. Mutation of single AIMs significantly compromised complementation in comparison to WT Exo70B2, and was mostly abrogated in the ΔAIM1/AIM2 double mutant (Figure 5B). To further characterize the interaction, we carried out in vitro pull-down assays with purified recombinant proteins. MBP-Exo70B2 was able to co-purify His-ATG8f, indicating that the proteins interact directly (Figure 5C).

The presence of AIMs in Exo70B2 suggested that they mediate its transport into the vacuole via autophagy. We transiently coexpressed Exo70B2 WT and the ΔAIM1/AIM2 variant with ATG8a and tested delivery into the vacuole in the presence of BTH and ConcA. As previously shown, Exo70B2 was autophagocytosed together with ATG8 (Figure 5D). However, the ΔAIM1/AIM2 mutant

remained outside of the vacuole, indicating that autophagy of Exo70B2 requires the presence of AIMs.

In contrast to AIM1, which is located in a highly variable region of the Arabidopsis Exo70 family, AIM2 is present in 65% of the Arabidopsis Exo70 homologues, as well as conserved in *Saccharomyces cerevisiae* Exo70 (Figure S4B). The conservation of the second AIM in the yeast Exo70, opened the possibility that the interaction with ATG8 and its transport into the vacuole, represent an ancestral function. We therefore generated a yeast strain expressing an Exo70-FLAG fusion protein from a genomic insertion and transformed these cells with a plasmid carrying GFP-ATG8. Under nutrient replete conditions Exo70 interacted with ATG8 (Figure S4C), and the interaction was markedly increased after 1h nitrogen (N) deprivation (Figure S4C). These results show that the interaction between Exo70 and ATG8 is conserved across kingdoms and that analogously to plants, the interaction with ATG8 uncovers a link to autophagy.

Notably, the identified MAPK-mediated phosphorylation sites are located in the vicinity of the AIMs, suggesting a potential role in their regulation (Figure 5A). To test whether phosphorylation had an impact on the interaction with ATG8, we also tested the non-phosphorylatable (S554/567A) and phospho-mimetic (S554/567D) variants of Exo70B2. Coexpression of ATG8 with S554/567A displayed a significantly decreased YFP complementation, when compared to S554/567D (Figure 5E and Figure S5A), suggesting that phosphorylation of serines increases Exo70B2's ability to interact with ATG8. We further confirmed these results by in vitro pull-down assays. In comparison to the S554/567A Exo70B2, ATG8 was co-precipitated more efficiently by the S554/567D phosphomimetic variant, suggesting a stronger interaction (Figure 5F). However, both mutant variants were still delivered to the vacuole (Figure S5B).

In order to obtain some insight into the possible mechanism by which phosphorylation of S554 and S567 influences ATG8 binding to the AIMs, we generated a structural model of Exo70B2's C-domain. Various crystal structures are available, including the Arabidopsis Exo70A1 homologue (Zhang et al., 2016). However, the model with the highest confidence was obtained using the yeast Exo70 structure (pdb 2pfv; Figure S6A) (Moore et al., 2007). Serine 554 is predicted to be positioned directly opposite and in close proximity to AIM1, opening the possibility that phosphorylation influences ATG8 binding by generating a negative charge that enhances affinity (Figure S6B). Serine 567, on the other hand, is positioned on the side opposite to the AIM2 docking surface, suggesting an allosteric effect when phosphorylated.

Together, we show that Exo70B2 autophagy requires its AIM motifs, and that phosphorylation at S554 and S567 may control ATG8 interaction.

Expression of Exo70B2 phosphonull variant enhances sensitivity to BTH and resistance to avirulent bacteria

Our results show that Exo70B2 is a substrate of autophagy, as reflected by the BTH-induced accumulation in the microsomal fraction. Moreover, activating the immune response by flg22 treatment induced the transport of Exo70B2 into the vacuole.

In order to investigate the function of Exo70B2 phosphorylation, we scored the impact of BTH on seedling root growth of *exo70* mutants, and lines complemented with WT, phosphonull or phosphomimetic Exo70B2 variants (Figure S7A and Figure S7B). BTH had little to no effect on root growth of Col-0 plants when compared with controls under the used conditions (Figure 6A and Table S2). Similarly, no major changes were observed for the other lines, with the exception of *exo70B2-3* plants complemented with WT Exo70B2 and the S554/567A phosphonull variant (Figure 6A and Table S2). Both transgenic lines expressing the WT and S554/567A Exo70B2 showed root growth inhibition in the presence of BTH. Of note, the S554/567A phosphonull mutant was significantly more sensitive than WT Exo70B2 expressing lines, displaying growth arrest after transplanting them onto BTH-containing media. By contrast, the S554/567D phosphomimetic variant showed no significant difference to the control (Figure 6A and Table S2). To compare the response to BTH we also tested the accumulation of PR1, a small secreted protein with antimicrobial activities. In agreement with the effect on root growth inhibition, PR1 accumulated at much higher levels in seedlings expressing the S554/567A phosphonull mutant after BTH treatment (Figure 6B).

Because BTH is an analogue of SA, a central defence hormone, these observations suggested that phosphorylation states of Exo70B2 may also affect plant immune responses. We subsequently carried out pathogen infection assays using the virulent *Pseudomonas syringae* pv. *tomato* DC3000 (*Pst*), as well as an avirulent *Pst* strain expressing the AvrRPS4 effector, which is recognized in Arabidopsis and activates effector-triggered immunity (ETI). As previously reported, *exo70B2-3* is more susceptible to the virulent *Pst* when compared to the WT Col-0 (Figure 6C). Re-introducing the *GFP-Exo70B2* complemented the enhanced susceptibility back to WT levels (Figure 6C). The S554/567A and S554/567D mutants however, also complemented the phenotype and displayed no differences to the WT. Nevertheless, lines transformed with the ΔC construct displayed *exo70B2-3* levels of susceptibility, indicating that the C-domain is required for Exo70B2 function in resistance to *Pst*.

Because the S554/567A variant conferred BTH hypersensitivity, we reasoned that Exo70B2 may also function in responses that induce the SA pathway. During ETI, plants trigger the hypersensitive response, which is a robust immune reaction characterized by programmed cell-death and the concomitant accumulation of high levels of SA (Jones and Dangl, 2006). In agreement with the enhanced sensitivity to BTH, growth of *Pst-AvrRPS4* was strongly reduced in plants expressing the S554/567A variant (Figure 6D). No significant differences were observed for the other lines.

These results demonstrate that mutating residues S554 and S567 to non-phosphorylatable alanines, renders plants more sensitive to BTH and results in an increased resistance during ETI. Hence, phosphorylation of Exo70B2 is potentially required to regulate processes triggered by BTH or SA.

Discussion

Exo70B2 and vesicle tethering

The canonical function of the exocyst complex is exocytosis by mediating early tethering of post-Golgi vesicles before SNARE-mediated membrane fusion. Recent studies indicate that the plant exocyst can mediate polarity of the ATP-binding cassette transporter PEN3 at the PM (Mao et al., 2016), and coordinate the transport of CASP1 to specific regions in the PM through the Exo70A1 subunit (Kalmbach et al., 2017). In line with these observations, our results indicate that Exo70B2 also locates to the PM in dynamic foci. Furthermore, the accumulation in BFA-compartments indicates that Exo70B2 transits through the TGN. This trait is, to the best of our knowledge, exclusive to Exo70B2, and suggests that it may have adopted unique features. The localization to the PM and accumulation in BFA-bodies reflect the canonical function of Exo70B2 in post-Golgi vesicle transport in secretion (Figure 1B, Figure 1C and Figure 7).

Additional roles of Exo70B2

It has become clear in recent years, that the exocyst is additionally involved in autophagy (Bodemann et al., 2011), but its exact roles still need to be defined. Several links have recently been reported connecting the exocyst, and more specifically its Exo70 subunits, to autophagy in plants. Here, we reveal that Exo70B2 possesses two AIMs located in the C-domain that mediate its transport into the vacuole by directly interacting with ATG8 for autophagy (Figure 4D). Similar to observations by Lin and colleagues (2015), we show that BTH induces the colocalization of Exo70B2 punctae with ATG8 and NBR1 (Figure 2B), and additionally, that flg22 treatment also results in Exo70B2 transport into the vacuole for degradation.

Moreover, we identify two phosphorylation sites located in the C-domain of Exo70B2. The C-domain of Exo70 subunits harbours the surface that mediate the interaction with phospholipids (He et al., 2007a; Mei et al., 2018). A conserved function of the C-domain in plants was indirectly demonstrated for Exo70A1, which is targeted by the small molecule Endosidin2. Binding of Endosidin2 to a pocket within the C-domain inhibits Exo70A1 function (Zhang et al., 2016).

There are two possible mutually nonexclusive scenarios by which phosphorylation of Exo70B2 may modulate its function. First, phosphorylation regulates Exo70B2 binding to the PM, therefore the phosphonull variant may be locked in its canonical secretory function. Identified sites are located in the C-domain, which mediates the interaction of Exo70 orthologues with PM phosphoinositides through ionic interactions (He et al., 2007a; Liu et al., 2007). Exo70B2 is predicted to possess polybasic

regions in the C-domain which could mediate interaction with phospholipids (Figure S9A) (Liu et al., 2007; Zhao et al., 2013; Pleskot et al., 2015). Phosphorylation sites (S554 and S567) are placed adjoining to the last stretch of a basic ridge (Figure S9A), opening the possibility that introduction of negative charges by phosphorylation modulates phospholipid binding.

In a second scenario, enhanced interaction with ATG8 may contribute in redirecting Exo70B2 into the autophagic pathway (Figure 7). S554 is predicted to be in close proximity to AIM1, opening the possibility that phosphorylation controls the interaction with ATG8 by generating a negatively-charged patch, known to increase ATG8 binding (Figure S6B) (Noda et al., 2010).

However, the mutant variant S554/567A was not significantly affected in its transport into the vacuole, indicating that phosphorylation may contribute to autophagy but is dispensable (Figure S5B). A possible reason for this observation is that Exo70B2 is delivered to the vacuole by an alternative pathway. Because Exo70B2 cycles between the PM and TGN, it may additionally enter the canonical endocytic degradation pathway. Indeed, a subpopulation of punctae did not colocalize with ATG8 (Figure 2B). In line with these observations, colocalization of Exo70E2 and ATG8e was significantly increased after longer BTH and ConcA treatments (Lin et al., 2015).

AIMs are typically found in autophagic receptors, such as NBR1, and act as tethers by additionally binding ubiquitinated substrates to mediate the association to autophagosomes, in a process termed selective autophagy (Kirkin et al., 2009; Svenning et al., 2011). The presence of AIMs in Exo70B2 suggests that it may additionally drive the transport of the associated exocyst complex. Supporting such a scenario, Exo70B2 binds to the core subunit Exo84 (Stegmann et al., 2012), and BTH treatment induced the accumulation of autophagosome-like compartments of the Sec6 subunit (Figure S1A).

Exo70B1 colocalization with ATG8 and the development of spontaneous cell death lesions before flowering are reminiscent of autophagy defective mutants. This has led to the hypothesis that it plays a general function in autophagy. However, a recent study revealed that *exo70B1*'s cell death phenotype is dependent on the truncated immune sensor TN2 (Zhao et al., 2015), putting into question the relation of Exo70B1's proposed general role in autophagy (Kulich et al., 2013). Other Arabidopsis *exo70* mutants also do not display typical autophagy deficiency phenotypes (Zhao et al., 2015). Therefore, Exo70 subunits in Arabidopsis are likely to act downstream of autophagy activation, where they are substrates and/or may mediate selective autophagy.

Interaction of yeast ATG8 and Exo70 indicates a across-kingdoms conservation, suggesting that this represents an ancestral function. Indeed, silencing of the human Exo70 did inhibit the formation of autophagosomes (Bodemann et al., 2011). Supporting a conserved role in autophagy, disruption of Arabidopsis and *Brassica napus* Exo70A1 function inhibits the formation of secretory vesicles and multivesicular bodies (MVBs) at zones of pollen reception in the stigma PM (Samuel et al., 2009; Safavian et al., 2015). Similarly, for self-incompatible pollinations, secretory vesicles and MVBs are

absent from the PM of stigmatic papillae, and autophagy appeared to be induced to redirect vesicles and MVBs to the vacuole (Safavian and Goring, 2013).

Exo70B2 and Immunity

The secretory pathway is intimately engaged in the immune response to pathogens. It mediates the delivery of both plasma membrane inherent proteins such as immune receptors and ABC-transporters such as FLS2 and PEN3, respectively (Dormann et al., 2014), as well as soluble proteins that are secreted into the apoplast such as PR1 (Kalde et al., 2007). As a component of the secretory machinery, several lines of evidence indicate that the exocyst plays a key role in plant immunity (Pecenkova et al., 2011; Stegmann et al., 2012; Ostertag et al., 2013; Stegmann et al., 2013; Fujisaki et al., 2015; Zhao et al., 2015), as well as in the innate immune system of mammals (Chien et al., 2006; Ishikawa et al., 2009).

Phosphorylation of Exo70B2 by MAPKs may act as a direct feed-back system to regulate secretory activity by acting as a rheostat to surveil cellular homeostasis. SA accumulation, or treatment with its analogue BTH, results in a massive increase of secretory activity (Wang et al., 2005; Nagashima et al., 2014). Importantly, upregulation by SA or BTH poses severe strains on the secretory pathway, causing cellular stress and activating responses that include the unfolded protein response to maintain homeostasis (Wang et al., 2005; Nagashima et al., 2014; Angelos et al., 2017). Such responses are conserved across kingdoms and are required to maintain and execute immune responses (Zhang et al., 2015; Grootjans et al., 2016). Thus, redirection of Exo70B2 into the vacuole for degradation may contribute to the downregulation of the secretory activity (Angelos et al., 2017). Accordingly, plants expressing the Exo70B2 S554/567A phosphonull variant were significantly more sensitive to BTH (Figure 6A) and more resistant to the avirulent *Pst* strain that triggered ETI (Figure 6D).

A caveat to this interpretation is that *exo70b2-3* complemented with a WT Exo70B2 also conferred BTH hypersensitivity, albeit significantly weaker than the S554/567A Exo70B2 variant. This observation possibly reflects an altered stoichiometry of Exo70B2 to kinases such as MPK3, leading to increased levels of non-phosphorylated Exo70B2 species that result in a phosphonull-like phenotype. Moreover, the inability of the phosphonull variant, but not of the phosphomimetic variant, to restrict the growth arrest response induced by BTH, underscores the importance of S554 and S567 phosphorylation.

Exo70B2 contributes to PTI (Figure 6C) (Stegmann et al., 2012), but mutation of the phosphorylation sites did not affect resistance to virulent bacteria suggesting mutant variants are still active. However, the C-terminus is indispensable for functionality since ΔC mutants did not complement the *exo70B2-3* phenotype (Figure 6C).

We previously showed that Exo70B2 is targeted by the E3 ubiquitin ligase PUB22, and is rapidly degraded in response to flg22 treatment (Stegmann et al., 2012). Here we show that Exo70B2 is

transported to the vacuole for degradation also after flg22 elicitation. While PUB22 mediates its own degradation through the proteasome (Furlan et al., 2017), it probably contributes to Exo70B2 degradation by modification with alternative types of ubiquitin chains. Lys63-linked chains are required for the degradation of membrane proteins (Leitner et al., 2012; Martins et al., 2015). This is supported by studies showing that PUB12 and PUB13 mediate the degradation of membrane proteins FLS2, BRI1, CERK1 and ABI1 (Lu et al., 2011; Kong et al., 2015; Liao et al., 2017; Zhou et al., 2018).

Conclusion

Together, our results suggest that Exo70B2 represents an intersection point in which immune signalling, secretory and autophagic pathways meet. It participates in two distinct cellular pathways, namely TGN-PM trafficking and autophagy. Our observations suggest that Exo70B2 phosphorylation may contribute to its redirection from TGN-PM trafficking into the autophagic pathway, which is required to control enhanced secretory activity induced by BTH and during ETI (Figure 7).

Materials and Methods

Plant materials and growth conditions

Arabidopsis thaliana (Col-0 accession) was used throughout this study. Seeds were surface sterilized and germinated on 1/2 Murashige Skoog media (pH 5.7) supplemented with 0.25% sucrose and 0.7% agar. Arabidopsis mutants *exo70b2-3* (GK726G07), *exo70b1-1* (GK114C03) (Stegmann et al., 2012) and *atg7-2* (GK-655B06) (Hofius et al., 2009) were previously described. All plants used for imaging were 4 day-old seedlings germinated under long day conditions (8h dark, 16 h light). Protoplasts were isolated from 5-week-old plants as described before (He et al., 2007b).

Pathogen Infection assays

For bacterial growth experiments, six-week old plants were spray inoculated with a solution of $5x10^8$ c.f.u./ml *Pseudomonas syringae* pv. *tomato* DC3000 (*Pst*) as previously described (Zipfel et al., 2004). Bacterial growth was measured 3 days after inoculation. For ETI, leaves were pressure-infiltrated with a solution of *Pst-AvrRPS4* $O.D._{600}$ 0.001, and bacterial growth was assessed 3 days after inoculation.

Protein purification and in vitro pull down

Recombinant MBP-Exo70B2, GST-MPK3 and GST-MPK6 were described previously (Stegmann et al., 2012). To generate recombinant His-ATG8f, coding sequence of ATG8f was cloned into pDEST17 by LR reaction. For in vitro pull-down, recombinant proteins were expressed in *Escherichia coli* after induction by 0.3mM at 28°C for 3-4h. To extract recombinant proteins, *E. coli* pellets from 50ml cultures were sonicated in 10ml column buffer (20mM Tris-HCl pH7.4, 200mM NaCl, 1mM EDTA, 1mM DTT, 1mM PMSF, 0.5% v/v Triton X-100) and incubated at 4°C for 30 min. Extracted recombinant proteins were immobilized on either amylose or glutathione agarose resins. Thereafter, recombinant proteins of interacting candidates were added and incubated at room temperature for 1 h before washing, elution and analysed by immunoblotting.

In vitro phosphorylation assay

In vitro phosphorylation assays were performed in kinase buffer (20mM Hepes pH 7.5, 15mM MgCl2, 5mM EGTA, 1mM DTT, 0.1mM ATP, 2µCi [gamma-32P]ATP) using recombinant full length MBP-Exo70B2 and active GST-MPK3, GST-MPK4 and GST-MPK11 or non-tagged MPK6 (preactivation was performed using constitutively active PcMKK5-DD) (Lee et al., 2004). Samples were incubated for 30 min at 37 °C; reactions were stopped by addition of SDS-PAGE sample buffer and separated by 10 % SDS-PAGE. Gels were stained with Coomassie Brilliant Blue and analyzed by autoradiography.

Protein extraction and Immunoblot

To extract total proteins, 250mg fresh weight plant material was ground in liquid nitrogen to a fine powder and 2x volume buffer (10mM HEPES/KOH pH 7.5, 13.7% w/v sucrose, 5% glycerol and protease inhibitor cocktail) was added and ground to homogeneity. To obtain S10, S100 and P100 fractions, total proteins were centrifuged either for 5 min at 10k G (resulting supernatant is S10) or

30 min at 100k G (resulting supernatant and pellet are S100 and P100 fractions, respectively). Before resolving on SDS-PAGE, 1x volume of 2x Laemmli sample buffer was added to the protein and denatured at 68°C for 10min.

Root growth inhibition assays

To monitor impact of BTH on Arabidopsis root growth, 4-day old seedlings were transferred to 1/2 Murashige Skoog media (0.25% sucrose, pH 5.7) supplemented with 100mM BTH and incubated vertically under short day conditions (8h light/16h dark). Primary root length was measured after 7 days.

Life-imaging and Inhibitor treatment

All treatments were performed in 1/2 MS liquid media unless otherwise stated. To assay the increase in GFP-Exo70B2 fluorescence intensity, four-day old seedlings were incubated overnight in 100µM BTH. Quantification of increased fluorescence intensity (FI) signal was performed using Fiji ImageJ as described previously (McCloy et al., 2014). To visualize BFA compartments, seedlings were pre-stained with 5µM FM4-64 for 5min in dark followed by incubation in 50µM BFA for 45min. To quantify changes in Exo70B2 protein levels, seedlings were incubated overnight in 0.1% DMSO, 100µM BTH, 1µM ConcA, 50µM MG132 and 3h in 50µM CHX as well as indicated combinations. To visualize increased GFP-Exo70B2 and NBR1 levels, seven to ten-day old seedlings were treated for 3h with 1µM ConcA, 1h 1µM flg22 or in combination.

Subcellular localization GFP-Exo70B2 was visualized using the Zeiss LSM780n and LSM880 Airyscan laser scanning confocal microscope for high resolution images. GFP was exited using the 488 nm laser in conjunction with a 505-550 band-pass.

For Variable angle epifluorescence microscopy (VAEM), root hairs of Arabidopsis seedlings were imaged on a FEI More inverted wide field microscope (FEI, Germany) microscope using a 100 × 1.4 NA oil immersion objective. GFP was excited using a 488 nm solid-state laser diode. Fluorescence emission was collected with an EM-CCD camera with bandwidth filters ranging from 495–550 nm and fluorescence was collected with an acquisition time of 135 ms. Throughout image acquisition the microscope was operated in the 'TIRF' mode for vesicles in the evanescent field (the contact area between the root hair tip and the glass coverslip).

Quantitative BiFC

Five hundred µl of protoplasts from Col-0 or *exo70b2-3* plants were co-transformed with *pSPYNE-ATG8F* (10 µg) and either *pSPYCE-Exo70B2* (13µg), *pSPYCE-Exo70B2AA* (13µg), *pSPYCE-Exo70B2DD* (13µg), *pSPYCE-Exo70B2AIM1* (13µg), *pSPYCE-Exo70B2AIM2* (13µg), *pSPYCE-Exo70B2AIM1/2* (13µg) or empty *pSPYCE* vector (13µg). *mCherry* (7.2µg) was also co-transformed as an expression marker. Transformed protoplasts were incubated at room temperature for 14-16 h before CLSM imaging. Thirty images (with 25-40 transformed protoplast per image) were taken for each transformation

event and used for quantification. The percentage of transformed protoplast (as indicated by mCherry expression) that showed YFP complementation was scored manually.

Accession numbers

Sequence data from this article can be found in the Arabidopsis Genome Initiative under the following accession numbers: Exo70B2 (At1g07000); Exo70B1 (At5g58430); NBR1 (At4g24690); ATG8A (At4g21980); ATG8F (At4g16520); MPK3 (At3g45640); MPK4 (At4g01370); MPK6 (At2g43790); MPK11 (At1g01560).

Acknowledgments

The authors thank Deborah Gasperini for critical reading of the manuscript and all the members of the Trujillo laboratory for fruitful discussions and valuable comments. We thank Theresa Binder for help with the generation of the yeast strain. We are grateful for materials kindly provided by Viktor Zarsky *SEC6prom:SEC6-GFP* lines, Daniel Hofius anti-NBR1, Ken Shirasu anti-HSP90, Erika Isono *pENTR-ATG8f*, and to Steingrim Svenning and Terje Johansen for *pENTR-NBR1*.

List of Author contributions

O.K.T., C.W.L., P.M., T.K., G.F., M.Z., G.H., L.E.L., F.D. conducted experiments; T.O., W.H., J.L., M.T. designed experiments and analysed the data; M.T. wrote the paper

Funding information

This research was funded by the Leibniz association and the state of Saxony-Anhalt (O.K.T., G.F., P.M, W.H., M.Z. and M.T.), DFG SPP1212 (C.W.L.) and DFG SFB648 (J.L.).

Corresponding author email

mtrujillo@ipb-halle.de

Figure legends

Figure 1. Exo70B2 transits through the trans-Golgi network and localizes to the plasma membrane

(A) Confocal laser-scanning microscopy images of four-day old homozygous transgenic seedlings expressing GFP-Exo70B2 under the control of the constitutive promoter *UBQ10* in the *exo70b2-3* background. Shown are epidermal cells of cotyledons (top left) and roots (right) and transverse section of root (right bottom). Size bars represent 20µm (cotyledons) and 10µm (roots). **(B)**

UBQ10pro:GFP-Exo70B2/exo70b2-3 transgenic seedlings were incubated in 0.8M mannitol for 40 mins before analysed by CLSM. Plasmolysis is shown by the shrinking protoplasts. GFP-EXO70B2 is visible on the Hechtian strands indicated by arrowheads. Scale bar 10µm. **(C)** High-resolution microscopy pictures of *UBQ10pro:GFP-Exo70B2/exo70b2-3* transgenic seedling root hairs. Three optical sections are shown from root hair shaft to tip. Scale bar 10µm, V denotes vacuole **(D)** *UBQ10pro:GFP-Exo70B2/exo70b2-3* transgenic seedlings were stained with 5µM FM4-64 for 5 mins and subsequently incubated in 50µM BFA for 45 mins at room temperature. Scale bar 5µm.

Figure 2. Exo70B2 is transported into the vacuole and colocalizes with autophagic markers

(A) GFP-EXO70B2 is localised to autophagic body-like compartment after BTH and ConcA treatment. *UBQ10prom:GFP-Exo70B2/exo70b2-3* seedlings were treated o/n with either 0.1% DMSO, 1µM ConcA, 100µM BTH or 1µM ConcA + 100µM BTH. Confocal images of the same tissue were taken with identical imaging settings. Scale bars for cotyledon and root tissues are 20µm and 10µm respectively. **(B)** GFP-Exo70B2 colocalizes with autophagosome markers ATG8a and NBR1. Double transgenic lines carrying *UBQ10prom:GFP-Exo70B2* and *UBQ10prom:RFP-ATG8A* or *UBQ10prom:RFP-NBR1* were treated overnight with 1µM ConcA + 100µM BTH before CLSM analysis. Scale bar 10µm. **(C)** Co-localisation analysis for GFP-Exo70B2 with mCherry-ARG8 or mcherry-NBR1. Data points represent the technical replicates of 2 independent experiments. Boxplots show median and inter quantile range (IQR), outliers (> 1.5 times IQR) are shown as circles. **(D)** *UBQ10pro:GFP-Exo70B2/exo70b2-3* transgenic seedlings were treated with 0.1% DMSO (control), 100µM BTH overnight (o/n), 1µM ConcA o/n and indicated combinations and 50µM MG132. Samples from the same experiment were aliquoted, and total protein (detergent-solubilized) or soluble and microsomal fraction (supernatant from centrifugation step 5' at 12k rcf) were resolved by PAGE and analysed by IB using anti-GFP antibodies (shown are two cropped sections of the same blot). Equal loading is shown by CBB staining. Similar results were obtained in three biological replicates. **(E)** Total protein, soluble and microsomal fractions from *UBQ10pro:GFP-Exo70B2/exo70b2-3* transgenic seedlings were resolved by PAGE and analysed by IB using the indicated antibodies. Shown are equivalent protein amounts from different fractions. Plasma membrane intrinsic protein2 (PIP2) and heat shock protein 90 (HSP90) were used as markers for microsomal and soluble fractions, respectively. **(F)** Soluble and microsomal fractions of *UBQ10pro:GFP-Exo70B2/exo70b2-3* seedlings were analysed by IB after 100µM BTH o/n treatment. (F and G) Experiments were repeated with similar results.

Figure 3. Exo70B2 is degraded during the immune response via the vacuole

(A) *UBQ10prom:GFP-Exo70B2/exo70b2-3* seedlings were treated with 1µM flg22 (1h), 1µM ConcA (2h) or 1µM flg22 (1h) + 1µM ConcA (2h) and subsequently stained for 5 mins in 5µM FM4-64. Arrowheads

565 indicate vacuolar GFP-Exo70B2. Scale bar 5µm. **(B)** Two weeks old *UBQ10prom:GFP-*
566 *Exo70B2/exo70b2-3* seedlings were treated with 1µM flg22 for the indicated times. Samples were
567 mock treated (control) or 1µM ConcA was added 1h before elicitation with flg22. Total protein
568 fractions were analysed by IB using the indicated antibody (shown are two cropped sections of the
569 same blot).
570
571 **Figure 4. EXO70B2 is phosphorylated at residues S554 and S567.**
572 **(A)** Interaction between Exo70B2 and MPK3 detected by BiFC in Arabidopsis protoplasts. nYFP-
573 MPK3, nYFP-MPK6 or nYFP-MPK11 were coexpressed with cYFP-Exo70B2 as indicated. Free mCherry
574 was coexpressed to label the cytoplasm and nucleus. Scale bar 50µm. Experiment was repeated with
575 similar results. **(B)** Transgenic seedlings carrying *UBQ10prom:GFP-Exo70B2* were treated with 1µM
576 flg22 for 20min and the S10 protein fraction (input) was subjected to IP with anti-GFP beads.
577 Endogenous coimmunoprecipitated MPK3 was detected with MPK3-antibodies. **(C)** MBP-Exo70B2
578 pull-down assay using purified GST-MPK3 and GST-MPK6 on glutathione agarose beads as baits.
579 White arrows indicate autophosphorylated kinases **(D)** GST- Exo70B2 was incubated alone or with
580 activated GST-MPK3, GST-MPK4 and untagged MPK6 (white arrowheads). MPK11 could not be
581 activated by MKK5. Phosphorylation was visualized with ProQ Diamond stain. **(E)** Cartoon depicting
582 the localization of phosphorylated sites in Exo70B2 identified by LC-MS/MS from in vitro
583 phosphorylation assays with GST-MPK3 and in vivo from GFP-Exo70B2 immunopurified from
584 transgenic lines treated with flg22.
585
586 **Figure 5. Exo70B2 interacts with ATG8 via C-terminal AIMs**
587 **(A)** Cartoon depicting the localization and sequences of ATG8-interacting motifs (AIMs) highlighted
588 in violet. Phosphorylation sites are highlighted in red. **(B)** BiFC of coexpressed nYFP-ATG8F and
589 either cYFP-Exo70B2 (WT) or mutant variants cYFP-Exo70B2-ΔAIM1 (ΔAIM1), cYFP-Exo70B2-ΔAIM2
590 (ΔAIM2), cYFP-Exo70B2-ΔAIM1/AIM2 (ΔAIM1/2) or empty pSPYCE. Conctructs were transiently
591 coexpressed in Arabidopsis mesophyll protoplasts. mCherry was transformed as a marker for
592 transformation. Boxplots show median and inter quantile range (IQR), outliers (> 1.5 times IQR) are
593 shown as circles. Percentages of fluorescence complementation obtained from 30 independent
594 images, each with 25-40 transformed protoplasts. Total protoplasts scored for WT, ΔAIM1, ΔAIM2,
595 ΔAIM1/2 and empty vector were 723, 754, 708, 683 and 542, respectively. The experiment was
596 repeated with similar results. **(C)** Pull-down (PD) assay with recombinant His-ATG8f co-purified using
597 MBP-Exo70B2 on amylose agarose beads. Asterisk indicates MBP-Exo70B2. **(D)** Transport into the
598 vacuole was tested by coexpressing ATG8a and Exo70B2 or Exo70B2-ΔAIM1/2 transiently in
599 Arabidopsis mesophyll protoplasts form *exo70b2-3* plants. To visualize GFP-Exo70B2 transported

into the vacuole, protoplasts were treated with 1µM ConcA + 100µM BTH at room temperature for 14h before CLSM imaging. Scale bar 10 µm. **(E)** BiFC of coexpressed nYFP-ATG8F and either cYFP-Exo70B2 S554/567A (AA), S554/567D (DD) or empty vector were transiently coexpressed in Arabidopsis mesophyll protoplasts. mCherry was used as a transformation marker. Percentage of fluorescence complementation was evaluated as in **(B)**. Total protoplasts scored for Exo70B2 WT, AA, DD and empty vector were 1283, 695, 1325 and 1302, respectively. The experiment was repeated with similar results. **(F)** Pull-down assay using recombinant His-ATG8F co-purified with S554/567A (AA) or S554/567D (DD) MBP-Exo70B2 on amylose agarose beads. Asterisk indicates MBP-Exo70B2.

Figure 6. Plants expressing Exo70B2 phosphonull variant are more sensitive to BTH and resistant to avirulent bacteria

(A) Primary root lengths of *UBQ10pro:GFP-Exo70B2/exo70b2-3* transgenic seedlings expressing GFP-Exo70B2 WT, S554/567A (AA), S554/567D (DD) and ΔC-domain (ΔC) measured seven days after transplanting onto media +/-100µM BTH. Boxplots show median and IQR, outliers (> 1.5 times IQR) are shown as circles. Values of a representative experiment. Asterisk indicate statistically significant differences between control and BTH treatment (One-Way ANOVA and Tukey post hoc test, $p < 0.05$). Experiment was repeated four times with similar results. See also Table S2 for complete statistical analysis results. **(B)** Transgenic seedlings described in (A) were treated with 100µM BTH overnight (o/n). Total protein samples were resolved by PAGE and analysed by IB using anti-PR1 antibodies. Equal loading is shown by CBB staining. The experiment was repeated with similar results. **(C)** Infection assays with the virulent bacterial pathogen *Pseudomonas syringae* pv. *tomato* DC3000 (*Pst*) empty vector. Six week-old plants were spray inoculated with a bacterial suspension of $5x10^8$ c.f.u./mL and analysed 0 and 3 days after inoculation. Data shown as mean +/- S.D. (n = 5). Letters indicate statistically significant differences between c.f.u. in different lines three days after inoculation (dai, One-Way ANOVA and Tukey post hoc test, $p < 0.05$). Similar results were obtained in three independent experiments. **(D)** Infection assays with the avirulent bacterial pathogen *Pseudomonas syringae* pv. *tomato* DC3000 *AvrRPS4*. Six week-old plants were syringe-infiltrated with a bacterial suspension $O.D._{600}$ 0.001 and analysed 0 and 3 days after inoculation. Data shown as mean +/- S.D. (n = 5). Letters indicate statistically significant differences (One-Way ANOVA and Tukey post hoc test, $p < 0.05$).

Figure 7. Working model for the regulation of Exo70B2 function by phosphorylation.

Exo70B2 cycles between PM and the TGN under basal conditions, and upon BTH treatment, its transport into the vacuole by autophagy is increased. Phosphorylated Exo70B2 is autophagocytosed by interacting with ATG8.

Literature Cited

Angelos, E., Ruberti, C., Kim, S.J., and Brandizzi, F. (2017). Maintaining the factory: the roles of the unfolded protein response in cellular homeostasis in plants. Plant J **90,** 671-682.

Bethke, G., Pecher, P., Eschen-Lippold, L., Tsuda, K., Katagiri, F., Glazebrook, J., Scheel, D., and Lee, J. (2012). Activation of the Arabidopsis thaliana mitogen-activated protein kinase MPK11 by the flagellin-derived elicitor peptide, flg22. Mol Plant Microbe Interact **25,** 471-480.

Bodemann, B.O., Orvedahl, A., Cheng, T., Ram, R.R., Ou, Y.H., Formstecher, E., Maiti, M., Hazelett, C.C., Wauson, E.M., Balakireva, M., Camonis, J.H., Yeaman, C., Levine, B., and White, M.A. (2011). RalB and the exocyst mediate the cellular starvation response by direct activation of autophagosome assembly. Cell **144,** 253-267.

Chien, Y., Kim, S., Bumeister, R., Loo, Y.M., Kwon, S.W., Johnson, C.L., Balakireva, M.G., Romeo, Y., Kopelovich, L., Gale, M., Jr., Yeaman, C., Camonis, J.H., Zhao, Y., and White, M.A. (2006). RalB GTPase-mediated activation of the IkappaB family kinase TBK1 couples innate immune signaling to tumor cell survival. Cell **127,** 157-170.

Cole, R.A., Synek, L., Zarsky, V., and Fowler, J.E. (2005). SEC8, a subunit of the putative Arabidopsis exocyst complex, facilitates pollen germination and competitive pollen tube growth. Plant Physiol **138,** 2005-2018.

Cvrckova, F., and Zarsky, V. (2013). Old AIMs of the exocyst: evidence for an ancestral association of exocyst subunits with autophagy-associated Atg8 proteins. Plant Signal Behav **8,** e27099.

Cvrckova, F., Grunt, M., Bezvoda, R., Hala, M., Kulich, I., Rawat, A., and Zarsky, V. (2012). Evolution of the Land Plant Exocyst Complexes. Front Plant Sci **3,** 159.

Dormann, P., Kim, H., Ott, T., Schulze-Lefert, P., Trujillo, M., Wewer, V., and Huckelhoven, R. (2014). Cell-autonomous defense, re-organization and trafficking of membranes in plant-microbe interactions. New Phytol **204,** 815-822.

Fujisaki, K., Abe, Y., Ito, A., Saitoh, H., Yoshida, K., Kanzaki, H., Kanzaki, E., Utsushi, H., Yamashita, T., Kamoun, S., and Terauchi, R. (2015). Rice Exo70 interacts with a fungal effector, AVR-Pii, and is required for AVR-Pii-triggered immunity. Plant J **83,** 875-887.

Furlan, G., Nakagami, H., Eschen-Lippold, L., Jiang, X., Majovsky, P., Kowarschik, K., Hoehenwarter, W., Lee, J., and Trujillo, M. (2017). Changes in PUB22 Ubiquitination Modes Triggered by MITOGEN-ACTIVATED PROTEIN KINASE3 Dampen the Immune Response. The Plant Cell **29,** 726-745.

Grefen, C., Donald, N., Hashimoto, K., Kudla, J., Schumacher, K., and Blatt, M.R. (2010). A ubiquitin-10 promoter-based vector set for fluorescent protein tagging facilitates temporal stability and native protein distribution in transient and stable expression studies. Plant J. **64,** 355-365.

Grootjans, J., Kaser, A., Kaufman, R.J., and Blumberg, R.S. (2016). The unfolded protein response in immunity and inflammation. Nat Rev Immunol **16,** 469-484.

Gu, Y., Zavaliev, R., and Dong, X. (2017). Membrane Trafficking in Plant Immunity. Mol Plant **10,** 1026-1034.

He, B., Xi, F., Zhang, X., Zhang, J., and Guo, W. (2007a). Exo70 interacts with phospholipids and mediates the targeting of the exocyst to the plasma membrane. EMBO J **26,** 4053-4065.

He, P., Shan, L., and Sheen, J. (2007b). The use of protoplasts to study innate immune responses. Methods Mol Biol **354,** 1-9.

Hofius, D., Schultz-Larsen, T., Joensen, J., Tsitsigiannis, D.I., Petersen, N.H., Mattsson, O., Jorgensen, L.B., Jones, J.D., Mundy, J., and Petersen, M. (2009). Autophagic components contribute to hypersensitive cell death in Arabidopsis. Cell **137,** 773-783.

Honkanen, S., and Dolan, L. (2016). Growth regulation in tip-growing cells that develop on the epidermis. Curr Opin Plant Biol **34,** 77-83.

Ichimura, Y., Kirisako, T., Takao, T., Satomi, Y., Shimonishi, Y., Ishihara, N., Mizushima, N., Tanida, I., Kominami, E., Ohsumi, M., Noda, T., and Ohsumi, Y. (2000). A ubiquitin-like system mediates protein lipidation. Nature **408,** 488-492.

Ishikawa, H., Ma, Z., and Barber, G.N. (2009). STING regulates intracellular DNA-mediated, type I interferon-dependent innate immunity. Nature **461,** 788-792.

Jones, J.D., and Dangl, J.L. (2006). The plant immune system. Nature **444,** 323-329.

Kalde, M., Nuhse, T.S., Findlay, K., and Peck, S.C. (2007). The syntaxin SYP132 contributes to plant resistance against bacteria and secretion of pathogenesis-related protein 1. Proc Natl Acad Sci U S A **104,** 11850-11855.

Kalmbach, L., Hematy, K., De Bellis, D., Barberon, M., Fujita, S., Ursache, R., Daraspe, J., and Geldner, N. (2017). Transient cell-specific EXO70A1 activity in the CASP domain and Casparian strip localization. Nat Plants **3,** 17058.

Kirkin, V., Lamark, T., Sou, Y.S., Bjorkoy, G., Nunn, J.L., Bruun, J.A., Shvets, E., McEwan, D.G., Clausen, T.H., Wild, P., Bilusic, I., Theurillat, J.P., Overvatn, A., Ishii, T., Elazar, Z., Komatsu, M., Dikic, I., and Johansen, T. (2009). A role for NBR1 in autophagosomal degradation of ubiquitinated substrates. Mol Cell **33,** 505-516.

Kong, L., Cheng, J., Zhu, Y., Ding, Y., Meng, J., Chen, Z., Xie, Q., Guo, Y., Li, J., Yang, S., and Gong, Z. (2015). Degradation of the ABA co-receptor ABI1 by PUB12/13 U-box E3 ligases. Nat Commun **6,** 8630.

Kulich, I., Pecenkova, T., Sekeres, J., Smetana, O., Fendrych, M., Foissner, I., Hoftberger, M., and Zarsky, V. (2013). Arabidopsis exocyst subcomplex containing subunit EXO70B1 is involved in autophagy-related transport to the vacuole. Traffic (Copenhagen, Denmark) **14,** 1155-1165.

Lassowskat, I., Bottcher, C., Eschen-Lippold, L., Scheel, D., and Lee, J. (2014). Sustained mitogen-activated protein kinase activation reprograms defense metabolism and phosphoprotein profile in Arabidopsis thaliana. Front Plant Sci **5,** 554.

Lee, J., Rudd, J.J., Macioszek, V.K., and Scheel, D. (2004). Dynamic changes in the localization of MAPK cascade components controlling pathogenesis-related (PR) gene expression during innate immunity in parsley. J. Biol. Chem. **279,** 22440-22448.

Lee, J., Eschen-Lippold, L., Lassowskat, I., Bottcher, C., and Scheel, D. (2015). Cellular reprogramming through mitogen-activated protein kinases. Front Plant Sci **6,** 940.

Leitner, J., Petrasek, J., Tomanov, K., Retzer, K., Parezova, M., Korbei, B., Bachmair, A., Zazimalova, E., and Luschnig, C. (2012). Lysine63-linked ubiquitylation of PIN2 auxin carrier protein governs hormonally controlled adaptation of Arabidopsis root growth. Proc Natl Acad Sci U S A **109,** 8322-8327.

Li, S., van Os, G.M., Ren, S., Yu, D., Ketelaar, T., Emons, A.M., and Liu, C.M. (2010). Expression and functional analyses of EXO70 genes in Arabidopsis implicate their roles in regulating cell type-specific exocytosis. Plant Physiol **154,** 1819-1830.

Liao, D., Cao, Y., Sun, X., Espinoza, C., Nguyen, C.T., Liang, Y., and Stacey, G. (2017). Arabidopsis E3 ubiquitin ligase PLANT U-BOX13 (PUB13) regulates chitin receptor LYSIN MOTIF RECEPTOR KINASE5 (LYK5) protein abundance. New Phytol.

Lin, Y., Ding, Y., Wang, J., Shen, J., Kung, C.H., Zhuang, X., Cui, Y., Yin, Z., Xia, Y., Lin, H., Robinson, D.G., and Jiang, L. (2015). Exocyst-Positive Organelles and Autophagosomes Are Distinct Organelles in Plants. Plant Physiol **169,** 1917-1932.

Liu, J., Zuo, X., Yue, P., and Guo, W. (2007). Phosphatidylinositol 4,5-bisphosphate mediates the targeting of the exocyst to the plasma membrane for exocytosis in mammalian cells. Mol Biol Cell **18,** 4483-4492.

Lu, D., Lin, W., Gao, X., Wu, S., Cheng, C., Avila, J., Heese, A., Devarenne, T.P., He, P., and Shan, L. (2011). Direct ubiquitination of pattern recognition receptor FLS2 attenuates plant innate immunity. Science **332,** 1439-1442.

Mao, H., Nakamura, M., Viotti, C., and Grebe, M. (2016). A Framework for Lateral Membrane Trafficking and Polar Tethering of the PEN3 ATP-Binding Cassette Transporter. Plant Physiol **172,** 2245-2260.

Marshall, R.S., Li, F., Gemperline, D.C., Book, A.J., and Vierstra, R.D. (2015). Autophagic Degradation of the 26S Proteasome Is Mediated by the Dual ATG8/Ubiquitin Receptor RPN10 in Arabidopsis. Mol. Cell **58,** 1053-1066.

Martins, S., Dohmann, E.M., Cayrel, A., Johnson, A., Fischer, W., Pojer, F., Satiat-Jeunemaitre, B., Jaillais, Y., Chory, J., Geldner, N., and Vert, G. (2015). Internalization and vacuolar targeting of the brassinosteroid hormone receptor BRI1 are regulated by ubiquitination. Nat Commun **6,** 6151.

McCloy, R.A., Rogers, S., Caldon, C.E., Lorca, T., Castro, A., and Burgess, A. (2014). Partial inhibition of Cdk1 in G 2 phase overrides the SAC and decouples mitotic events. Cell Cycle **13,** 1400-1412.

Mei, K., Li, Y., Wang, S., Shao, G., Wang, J., Ding, Y., Luo, G., Yue, P., Liu, J.J., Wang, X., Dong, M.Q., Wang, H.W., and Guo, W. (2018). Cryo-EM structure of the exocyst complex. Nature structural & molecular biology.

Moore, B.A., Robinson, H.H., and Xu, Z. (2007). The crystal structure of mouse Exo70 reveals unique features of the mammalian exocyst. J Mol Biol **371,** 410-421.

Nagashima, Y., Iwata, Y., Ashida, M., Mishiba, K., and Koizumi, N. (2014). Exogenous salicylic acid activates two signaling arms of the unfolded protein response in Arabidopsis. Plant & cell physiology **55,** 1772-1778.

Noda, N.N., Ohsumi, Y., and Inagaki, F. (2010). Atg8-family interacting motif crucial for selective autophagy. FEBS Lett **584,** 1379-1385.

Novick, P., Field, C., and Schekman, R. (1980). Identification of 23 complementation groups required for post-translational events in the yeast secretory pathway. Cell **21,** 205-215.

Ostertag, M., Stammler, J., Douchkov, D., Eichmann, R., and Huckelhoven, R. (2013). The conserved oligomeric Golgi complex is involved in penetration resistance of barley to the barley powdery mildew fungus. Mol Plant Pathol **14,** 230-240.

Pecenkova, T., Hala, M., Kulich, I., Kocourkova, D., Drdova, E., Fendrych, M., Toupalova, H., and Zarsky, V. (2011). The role for the exocyst complex subunits Exo70B2 and Exo70H1 in the plant-pathogen interaction. J Exp Bot **62,** 2107-2116.

Pleskot, R., Cwiklik, L., Jungwirth, P., Zarsky, V., and Potocky, M. (2015). Membrane targeting of the yeast exocyst complex. Biochim Biophys Acta **1848,** 1481-1489.

Ren, J., and Guo, W. (2012). ERK1/2 regulate exocytosis through direct phosphorylation of the exocyst component Exo70. Dev Cell **22,** 967-978.

Safavian, D., and Goring, D.R. (2013). Secretory activity is rapidly induced in stigmatic papillae by compatible pollen, but inhibited for self-incompatible pollen in the Brassicaceae. PLoS One **8,** e84286.

Safavian, D., Zayed, Y., Indriolo, E., Chapman, L., Ahmed, A., and Goring, D.R. (2015). RNA Silencing of Exocyst Genes in the Stigma Impairs the Acceptance of Compatible Pollen in Arabidopsis. Plant Physiol **169,** 2526-2538.

Samuel, M.A., Chong, Y.T., Haasen, K.E., Aldea-Brydges, M.G., Stone, S.L., and Goring, D.R. (2009). Cellular pathways regulating responses to compatible and self-incompatible pollen in Brassica and Arabidopsis stigmas intersect at Exo70A1, a putative component of the exocyst complex. Plant Cell **21,** 2655-2671.

Stegmann, M., Anderson, R.G., Westphal, L., Rosahl, S., McDowell, J.M., and Trujillo, M. (2013). The exocyst subunit Exo70B1 is involved in the immune response of Arabidopsis thaliana to different pathogens and cell death. Plant Signal Behav **8,** e27421.

Stegmann, M., Anderson, R.G., Ichimura, K., Pecenkova, T., Reuter, P., Zarsky, V., McDowell, J.M., Shirasu, K., and Trujillo, M. (2012). The ubiquitin ligase PUB22 targets a subunit of the exocyst complex required for PAMP-triggered responses in Arabidopsis. Plant Cell **24,** 4703-4716.

Svenning, S., Lamark, T., Krause, K., and Johansen, T. (2011). Plant NBR1 is a selective autophagy substrate and a functional hybrid of the mammalian autophagic adapters NBR1 and p62/SQSTM1. Autophagy **7,** 993-1010.

Tateda, C., Zhang, Z., Shrestha, J., Jelenska, J., Chinchilla, D., and Greenberg, J.T. (2014). Salicylic acid regulates Arabidopsis microbial pattern receptor kinase levels and signaling. Plant Cell **26,** 4171-4187.

Tzfadia, O., and Galili, G. (2013). The Arabidopsis exocyst subcomplex subunits involved in a golgi-independent transport into the vacuole possess consensus autophagy-associated atg8 interacting motifs. Plant Signal Behav **8,** doi: 10 4161/psb 26732.

Vlot, A.C., Dempsey, D.A., and Klessig, D.F. (2009). Salicylic Acid, a multifaceted hormone to combat disease. Annu. Rev. Phytopathol. **47,** 177-206.

Wang, D., Weaver, N.D., Kesarwani, M., and Dong, X. (2005). Induction of protein secretory pathway is required for systemic acquired resistance. Science **308,** 1036-1040.

Wen, T.J., Hochholdinger, F., Sauer, M., Bruce, W., and Schnable, P.S. (2005). The roothairless1 gene of maize encodes a homolog of sec3, which is involved in polar exocytosis. Plant Physiol **138,** 1637-1643.

Wu, B., and Guo, W. (2015). The Exocyst at a Glance. J Cell Sci **128,** 2957-2964.

Yoshimoto, K., Jikumaru, Y., Kamiya, Y., Kusano, M., Consonni, C., Panstruga, R., Ohsumi, Y., and Shirasu, K. (2009). Autophagy negatively regulates cell death by controlling NPR1-dependent salicylic acid signaling during senescence and the innate immune response in Arabidopsis. The Plant cell **21,** 2914-2927.

Zhang, C., Brown, M.Q., van de Ven, W., Zhang, Z.M., Wu, B., Young, M.C., Synek, L., Borchardt, D., Harrison, R., Pan, S., Luo, N., Huang, Y.M., Ghang, Y.J., Ung, N., Li, R., Isley, J., Morikis, D., Song, J., Guo, W., Hooley, R.J., Chang, C.E., Yang, Z., Zarsky, V., Muday, G.K., Hicks, G.R., and Raikhel, N.V. (2016). Endosidin2 targets conserved exocyst complex subunit EXO70 to inhibit exocytosis. Proc Natl Acad Sci U S A **113,** E41-50.

Zhang, L., Chen, H., Brandizzi, F., Verchot, J., and Wang, A. (2015). The UPR branch IRE1-bZIP60 in plants plays an essential role in viral infection and is complementary to the only UPR pathway in yeast. PLoS Genet **11,** e1005164.

Zhao, T., Rui, L., Li, J., Nishimura, M.T., Vogel, J.P., Liu, N., Liu, S., Zhao, Y., Dangl, J.L., and Tang, D. (2015). A truncated NLR protein, TIR-NBS2, is required for activated defense responses in the exo70B1 mutant. PLoS Genet **11,** e1004945.

Zhao, Y., Liu, J., Yang, C., Capraro, B.R., Baumgart, T., Bradley, R.P., Ramakrishnan, N., Xu, X., Radhakrishnan, R., Svitkina, T., and Guo, W. (2013). Exo70 generates membrane curvature for morphogenesis and cell migration. Dev Cell **26,** 266-278.

Zhou, J., Liu, D., Wang, P., Ma, X., Lin, W., Chen, S., Mishev, K., Lu, D., Kumar, R., Vanhoutte, I., Meng, X., He, P., Russinova, E., and Shan, L. (2018). Regulation of Arabidopsis brassinosteroid receptor BRI1 endocytosis and degradation by plant U-box PUB12/PUB13-mediated ubiquitination. Proceedings of the National Academy of Sciences.

Zipfel, C., Robatzek, S., Navarro, L., Oakeley, E.J., Jones, J.D., Felix, G., and Boller, T. (2004). Bacterial disease resistance in Arabidopsis through flagellin perception. Nature **428,** 764-767.

826 Figure 1

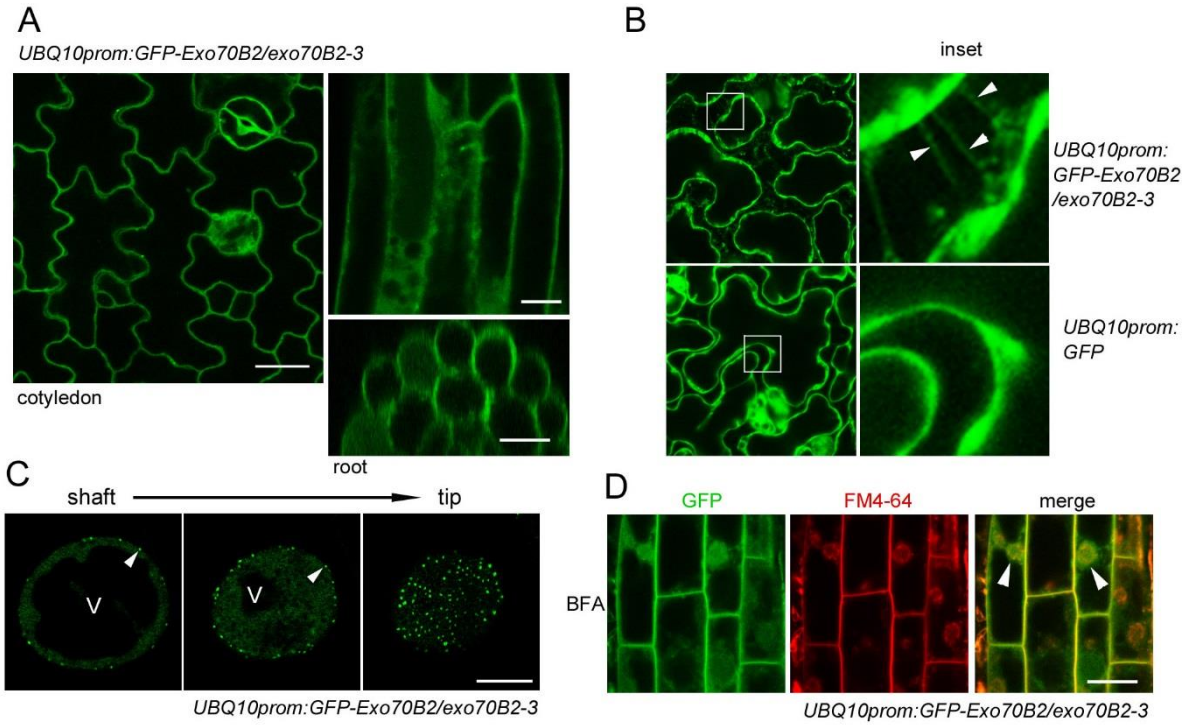

827

828 Figure 2

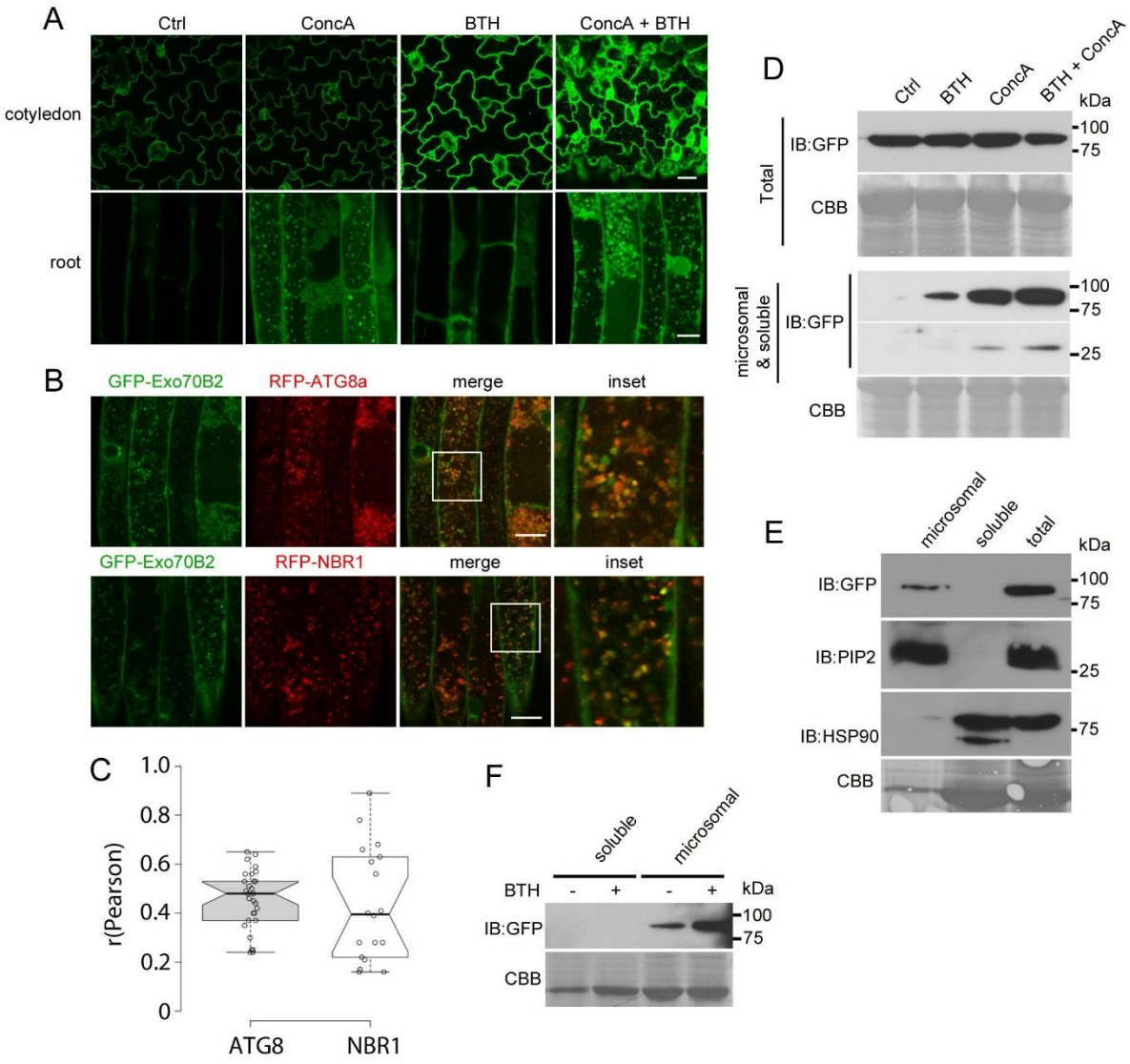

829

830 Figure 3

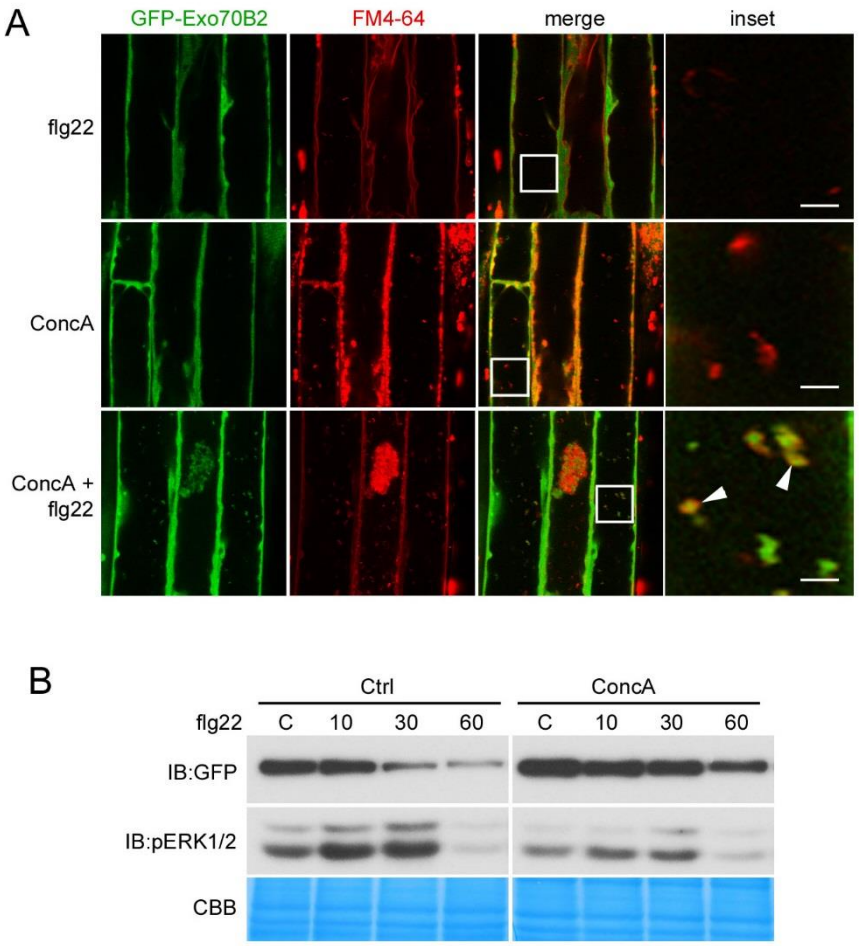

831

832 Figure 4

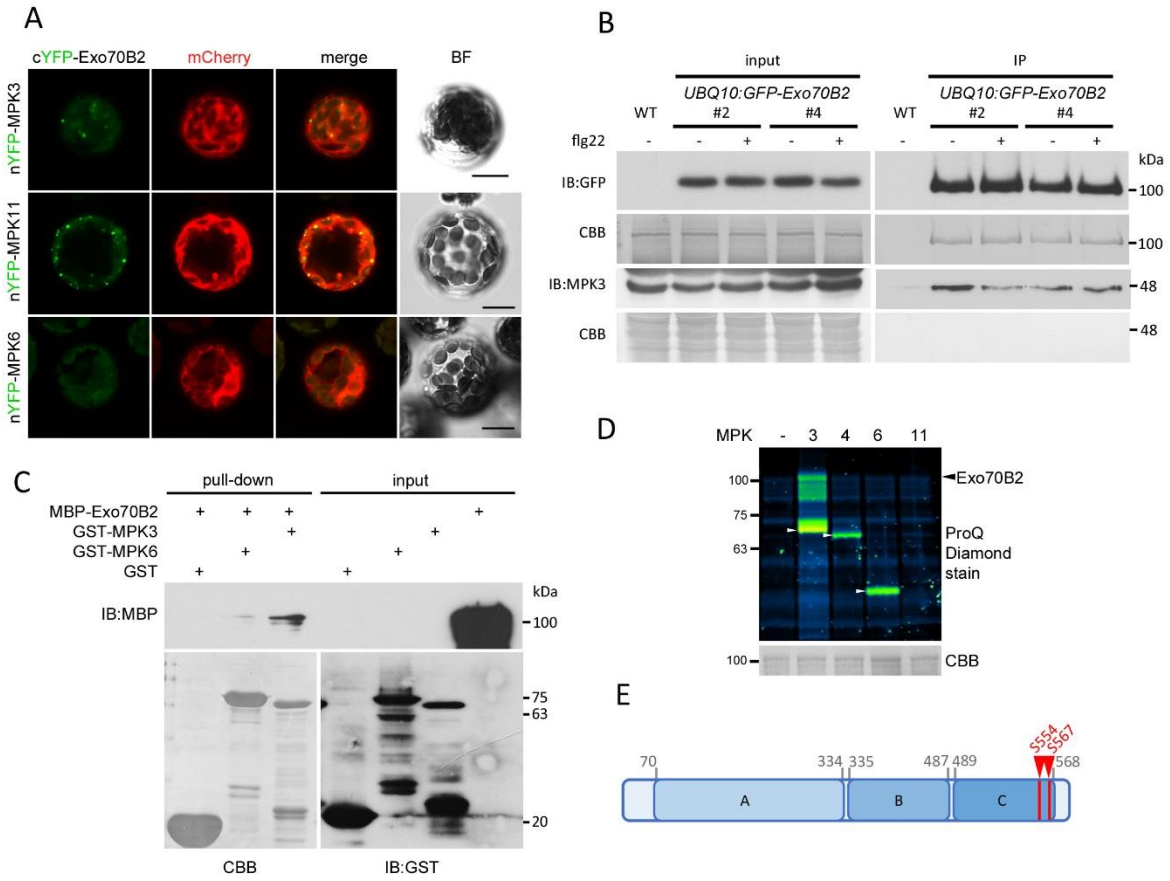

833

834 Figure 5

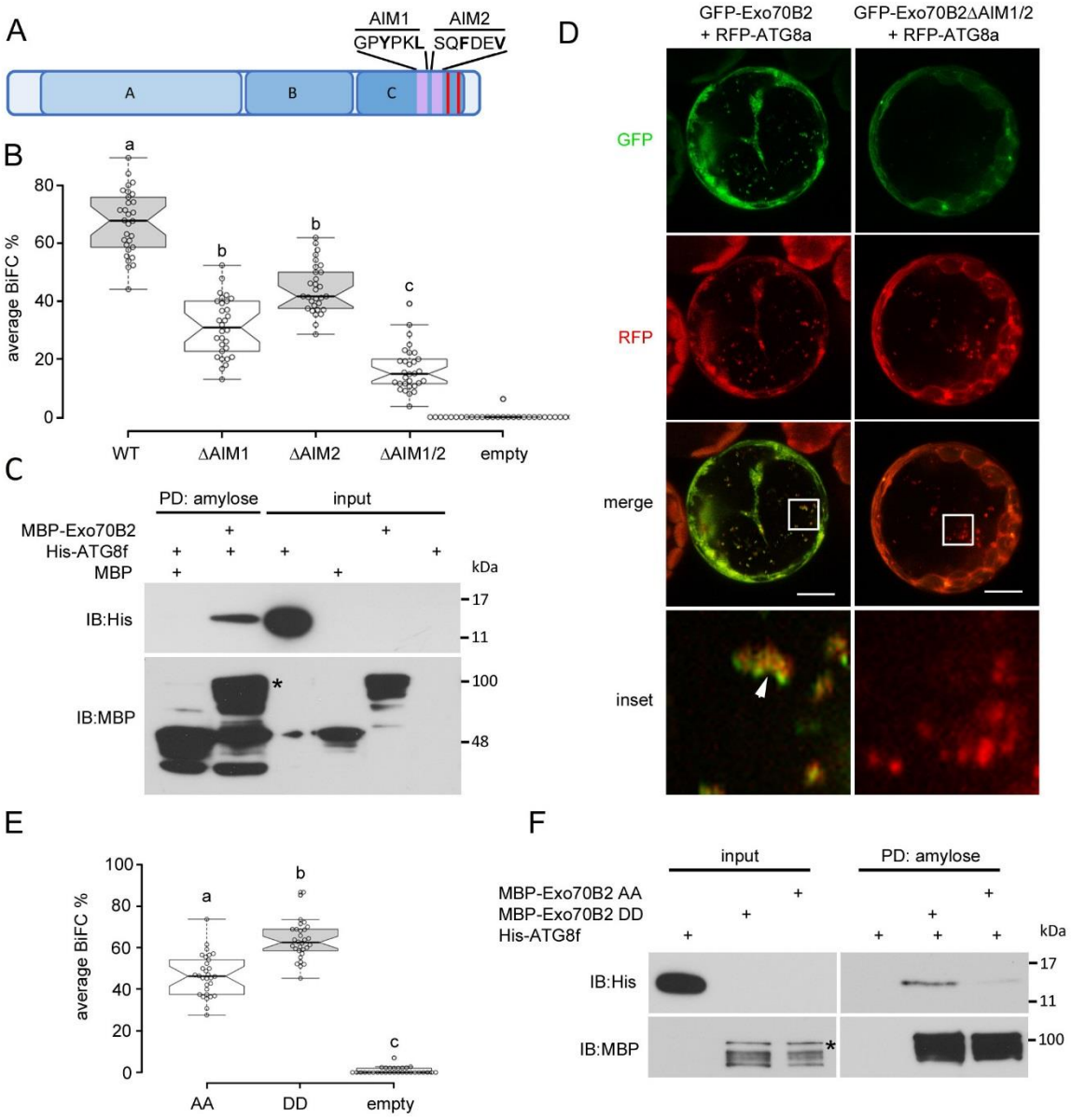

835

836 Figure 6

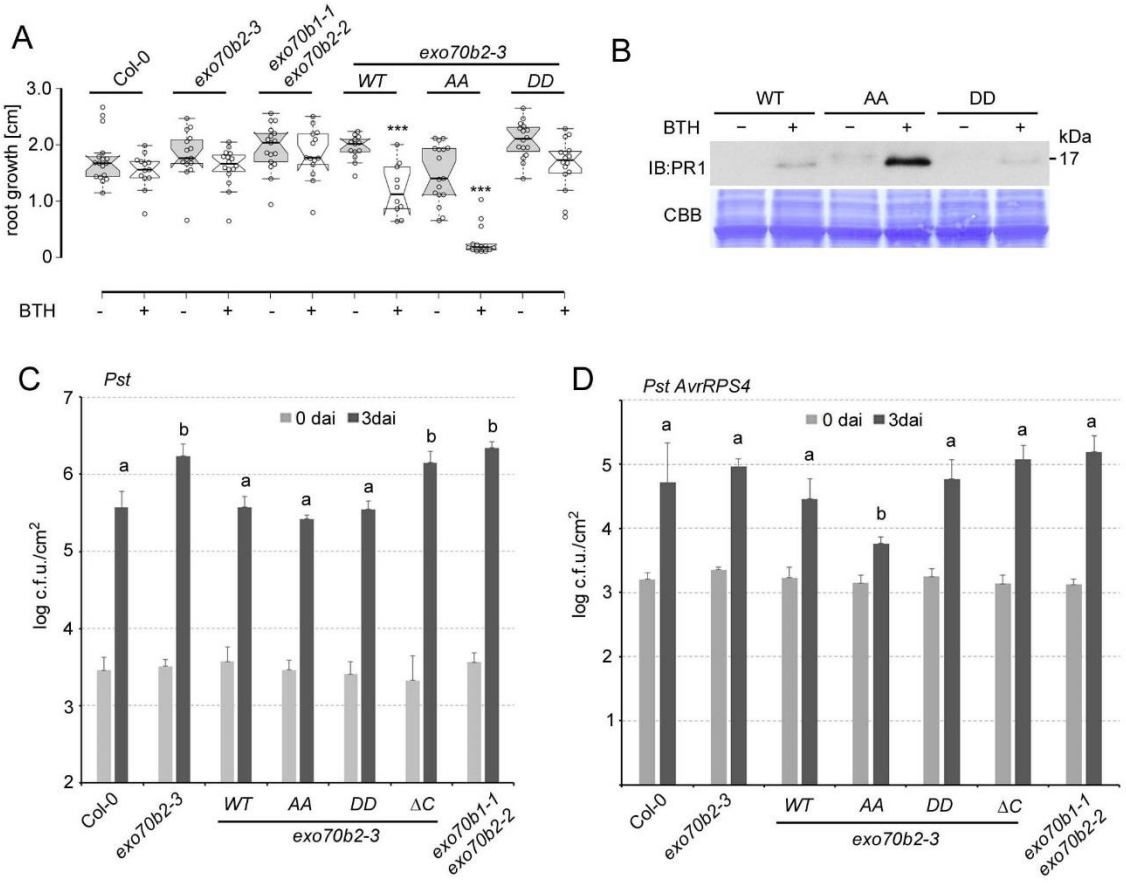

837

838 Figure 7

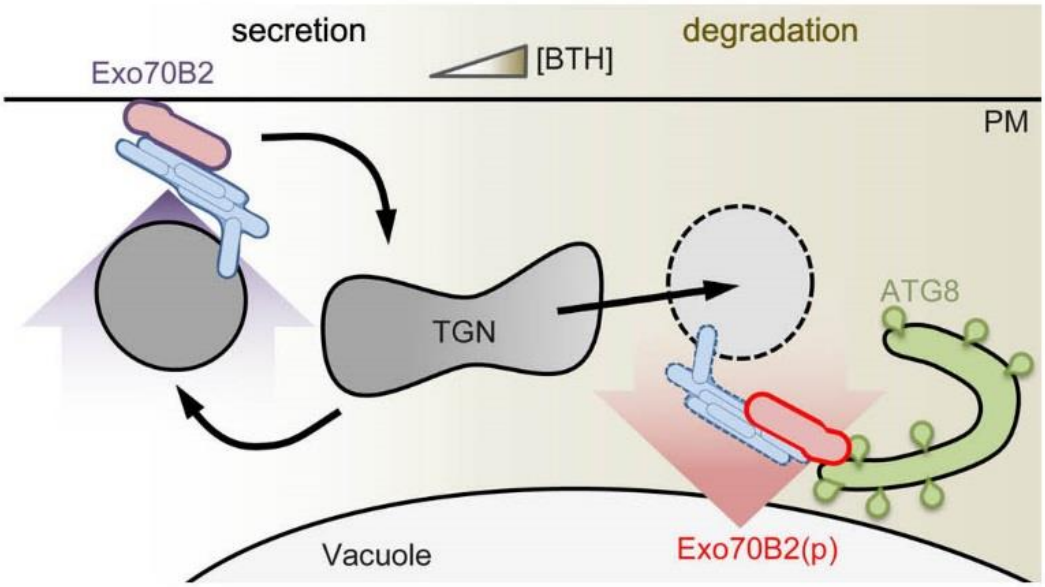

839